Hierarchical non-negative matrix factorization using multi-parametric MRI to assess tumor heterogeneity within gliomas.

Nicolas Sauwen[1,2], Diana Sima[1,2], Sofie Van Cauter[3], Jelle Veraart[4,5], Alexander Leemans[6], Frederik Maes[1,2], Uwe Himmelreich[7], and Sabine Van Huffel[1,2]

[1]Department of Electrical Engineering (ESAT), KU Leuven, Leuven, Belgium, [2]iMinds Medical IT, Leuven, Belgium, [3]Department of Radiology, University Hospitals of Leuven, Leuven, Belgium, [4]iMinds Vision Lab, Department of Physics, University of Antwerp, Antwerp, Belgium, [5]Center for Biomedical Imaging, Department of Radiology, New York University Langone Medical Center, New York, NY, United States, [6]Image Sciences Institute, University Medical Center Utrecht, Utrecht University, Utrecht, Netherlands, [7]Biomedical MRI/MoSAIC, Department of Imaging and Pathology, KU Leuven, Leuven, Belgium

Target audience: Clinicians and researchers interested in multi-parametric MRI (MP-MRI) for brain tumor diagnosis and follow-up.

Purpose: Advanced MR modalities such as Magnetic Resonance Spectroscopic Imaging (MRSI), perfusion-weighted MRI (PWI) and diffusion-weighted MRI (DWI) have shown their added value to non-invasively characterize brain tumors, detect full tumor extent and assess early success of therapy. Tissue characterization within gliomas is challenging due to the co-existence of several intra-tumoral tissue types within the same region and the high spatial heterogeneity in high-grade gliomas. Previous advanced MR studies have often simplified or neglected this aspect of tissue complexity. An accurate and reproducible method for brain tumor characterization and the detection of the relevant tumor substructures could be of great added value for the diagnosis, treatment planning and follow-up of individual patients.

Methods: ***Acquisition:*** 24 patients with primary glioma underwent MP-MRI, including conventional MRI (cMRI), PWI, MRSI and diffusion kurtosis imaging (DKI), (Philips Achieva 3T scanner). 11 patients were diagnosed with glioblastoma multiforme (GBM), 2 patients with anaplastic astrocytoma, 9 patients with a grade II glioma and 2 patients with grade I oligodendroglioma. cMRI consisted of T2 (TR/TE: 3000/80ms; slice/gap: 4/1 mm; turbo factor:10), T1 with contrast enhancement (TR/TE/TI: 9.7/4.6/900ms; flip angle: 8°; turbo field echo factor: 180) and FLAIR imaging (TR/TE/TI: 11000/120/2800 msec, slice/gap: 4/1 mm). Dynamic susceptibility contrast (DSC) MRI data were obtained using a gradient echo-EPI sequence (TR/TE: 1350/30ms; slice/gap: 3/0mm; 60 dynamic scans at 1s intervals). Cerebral blood volume (CBV) was calculated including leakage correction [1]. 2D-^{1}H MRSI was acquired with PRESS volume selection (TR/TE: 2000/35ms; section thickness: 10mm; receiver bandwidth: 2000Hz; samples: 2048; number of signal averages: 1; MOIST water suppression; pencil beam shimming; SENSE parallel imaging). AQSES-MRSI [2] was used for quantifying lipids (Lip), lactate (Lac), N-acetyl-aspartate (NAA), glutamine+glutamate (Glx), total creatine (Cre), total choline (Cho), myo-inositol (mI) and glycine (Gly). DKI was acquired using an EPI DWI sequence (b=0, 700, 1000 and 2800 in 10, 25, 40, and 75 uniformly distributed directions; TR/TE: 3200/90ms; d/D: 20/48.3ms; section thickness/gap: 2.5/0mm; SENSE parallel imaging). After motion and eddy current correction, diffusion and kurtosis tensors were estimated in each voxel using a constrained weighted linear least-squares algorithm [3]. Mean diffusivity (MD), fractional anisotropy (FA) and mean kurtosis (MK) maps were derived from the tensors. The diffusion maps were non-rigidly coregistered to the cMRI data to account for EPI distortion using ExploreDTI [4]. All other MR images were rigidly coregistered to the T1+contrast reference set using the normalized mutual information criterion. For MRSI, only one 2D slab was measured and only voxels within the MRSI region of interest could be analyzed.

hNMF analysis: Non-negative matrix factorization (NMF) approximately factorizes a matrix X into the product of a source matrix W and an abundance matrix H. The columns of W represent the sources and each column of H contains the abundance of the sources for one data point. In the case of our MP-MRI data, the rows of X represent the voxels and the columns represent the MP-MRI features. The sources correspond to different tissue types and each column of H contains the relative concentrations of the tissue types for one voxel. A hierarchical NMF (hNMF) algorithm was developed, consisting of 3 steps. In step1, 2-rank NMF is applied, resulting in a 'pathologic' and a 'normal' source and their abundance maps. In step2, NMF is applied to the pathologic and to the normal tissue region separately to find tissue-specific patterns. The sources are then re-combined in step3 using non-negative linear least squares fitting, to find the abundance maps. K-means clustering was applied to the abundance maps to obtain a tissue segmentation. Dice-scores were calculated with respect to a manual segmentation by a radiologist. Correlation coefficients were calculated between the pathologic tissue sources and the average feature vector within the corresponding tissue region. For the non-necrotic patients, Dice-scores and correlation coefficients were calculated for the whole tumor region, whereas for the GBM patients, validation scores are also reported for active tumor and necrosis separately. For comparison, the same hNMF analyses were also run when considering only cMRI data.

Results: Tables 1 and 2 report the Dice-scores and correlation coefficients for the non-necrotic patients and the GBM patients, respectively. Fig.1 shows some of the relevant MR parameters and the resulting abundance maps for active tumor and necrosis for a particular GBM patient.

		Dice-score tumor	Correlation coeff tumor
MP-MRI	Average	0.88	0.97
	Range	0.52 - 0.96	0.85 - 1
	Std dev	0.12	0.04
cMRI	Average	0.81	0.96
	Range	0.38 - 0.96	0.82 - 1
	Std dev	0.18	0.05

Table 1: Range, average and standard deviation of the Dice-scores and correlation coefficients of the non-necrotic patients for MP-MRI and cMRI only.

		Dice-score active tumor	Dice-score necrosis	Dice-score whole tumor	Correlation coeff active tumor	Correlation coeff necrosis
MP-MRI	Average	0.76	0.69	0.84	0.90	0.96
	Range	0.48 - 0.87	0.27 - 0.96	0.47 - 0.98	0.71 - 0.99	0.84 - 1
	Std dev	0.12	0.26	0.13	0.09	0.05
cMRI	Average	0.67	0.48	0.69	0.84	0.93
	Range	0.38 - 0.87	0.27 - 0.92	0.39 - 0.95	0.59 - 0.99	0.70 - 0.99
	Std dev	0.17	0.23	0.17	0.17	0.09

Table 2: Range, average and standard deviation of the Dice-scores and correlation coefficients for the GBM patients for MP-MRI and cMRI only.

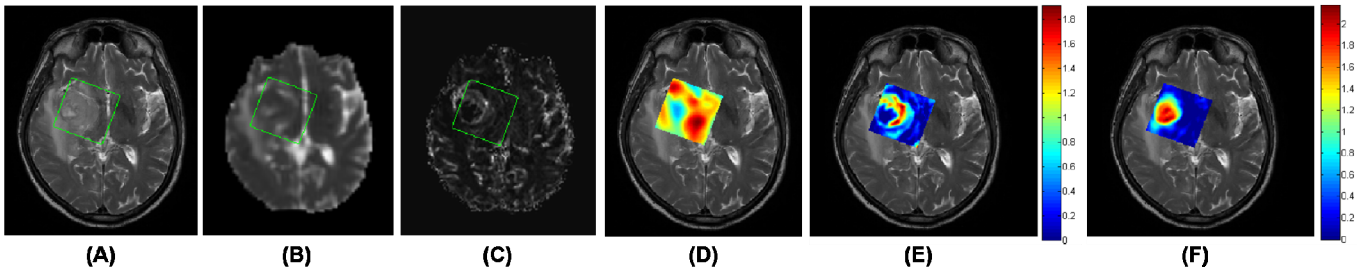

Fig.1: Coregistered MR parameter maps of different modalities for a GBM patient: T2 (A), MD (B), CBV (C) and Cre (D). The abundance maps after hNMF analysis are shown for active tumor (E) and necrosis (F).

Discussion: For MP-MRI, the average Dice-scores are higher than for state-of-the art supervised segmentation methods, which mostly use only cMRI data. For the non-necrotic tumors, the average Dice-score decreases by 7% when considering only cMRI data. For the GBM patients, a larger decrease in average Dice-scores is found: 9%, 21% and 15% for active tumor, necrosis and the whole tumor region, respectively. hNMF is therefore competitive as an unsupervised segmentation tool and the added value of using MP-MRI data has been shown. Average correlation coefficients are above 0.90 for MP-MRI, confirming that the sources can be considered as tissue-specific patterns. The hNMF method provides tissue characterization that goes beyond black-and-white segmentation. The abundance maps allow direct visual interpretation of the hNMF results, combining the information of all MP-MRI data into one map per tissue type. The relative contributions of different tissue types within the tumor region provide us with more insight in the tumor heterogeneity.

Conclusion: hNMF can be applied on a patient-by-patient basis, it does not require large training datasets nor data normalization and it provides a more refined tissue characterization compared to binary classification.

Acknowledgements: This work has been funded by: FWO G.0869.12N; IUAP P7/19/; FP7/2007-2013; EU MC ITN TRANSACT 2012 (n 316679).

References: [1] Boxerman JL, Schmainda KM, et al., AJNR Am. J. Neuroradiol. 2006;27:859–67. [2] Croitor Sava AR, Sima DM, et al., NMR Biomed. 2011;24:824–35. [3] Veraart J, Sijbers J, et al., NeuroImage 2013;81:335–346. [4] Leemans A, Jeurissen B, et al. Ann M Intl Soc Mag Reson Med. 2009; p. 3537.